

# Guaranteed obstacle avoidance of convex objects in 2D without object tracking, environment mapping, or stopping

Hasan A. Poonawala<sup>1</sup>

**Abstract**—This paper proves that a simple range-based end-to-end feedback controller avoids convex obstacles when its heading is sufficiently far away from a head-on collision. Sufficient is as small as nearly, but not exactly, 0 degrees for a wall or circular object and at least 45 degrees for any convex obstacle. The guarantees use a new modeling and analysis framework for sensor-object interaction combined with a new barrier function that are the main contributions. The controller avoids state estimation, mapping, object tracking, and learning from data. This guaranteed behavior is useful for navigating safely around arbitrary convex obstacles. We demonstrate the behavior of the controller in a simulated navigation scenario.

## I. INTRODUCTION

Mobile robots that can autonomously navigate human environments are a widely sought goal. Safe motion is critical for such robots. Algorithms for collision avoidance such as dynamic window approach (DWA) [1], vector polar histogram (VPH) [2], and follow-the-gap (FTG) [3] use 2D LiDAR for feedback without mapping, localization, or learning. These methods are typically effective, but lack guarantees or formal analysis. Navigation methods that use mapping [4], [5], localization [6], or learning [7], [8] are also effective, but they also lack guarantees and may be foiled by unpredictable edge cases.

Guarantees of safe motion are desirable but are currently difficult to obtain. Methods to obtain guarantees have two limitations: 1) they need access to an accurate environment model [9], [10] and/or 2) they involve solving partial differential inequalities [11]–[15], which is generally difficult and computationally expensive. These two properties together make guarantees currently impractical to obtain for mobile robots in dynamic, complex, or unseen environments.

Existing methods fail because safe decisions rely on being able to model the environment online (localization, local planning) or offline (stored maps or learning).

The main contribution of this work is to develop a model for object-sensor interactions that enables prediction of end-to-end controller behavior without requiring detailed object geometry information. This model enables proof of the ability of a simple controller to avoid arbitrary convex obstacles. A secondary contribution is to propose a barrier function for collision avoidance in terms of relative position variables to convex obstacles, and use it to derive a practical bound

This work was partially supported by the Department of Mechanical and Aerospace Engineering at the University of Kentucky.

<sup>1</sup>Hasan A. Poonawala is with the Department of Mechanical and Aerospace Engineering, University of Kentucky, Lexington, KY 40506, United States. E-mail: hasan.poonawala@uky.edu

condition which may be of separate interest. This guaranteed behavior is useful for navigating safely and competently in a wide range of environments. No state estimation, mapping, object tracking, or learning is needed. We view this simple controller as a reliable low-level reactive end-to-end controller that adds virtually no latency between sensing and action. Such low-level controllers enable execution of higher-level decisions, perhaps through a subsumption-like architecture [16]. They also enable safe exploration during learning for navigation.

The paper is organized as follows. Section II describes the mobile robot and sensor, Section III gives the problem statement, and Section IV describes the proposed controller. Section V uses a barrier function to provide a condition on a kinematic controller that guarantees collision avoidance. Section VI provides the main result: a formal analysis that the proposed closed-loop behavior meets the conditions in Section V. Section VII shows the performance of the proposed controllers in simulations. We end with a discussion of the limitations of the framework and potential future directions.

## II. RANGE-BASED NAVIGATION IN THE PLANE

This section describes the mobile robot model and sensors that this paper considers.

a) *Mobile Robots*: We consider kinematic models of mobile robots with control inputs as a linear speed  $v$  along a heading direction, and the rate of change  $\omega$  of that heading direction. If the pose  $\mathbf{x} \in \text{SE}(2)$  of the mobile robot is  $\mathbf{x} = (x, y, \varphi)$ , then

$$\dot{x} = v \cos \varphi, \quad \dot{y} = v \sin \varphi, \quad \dot{\varphi} = \omega. \quad (1)$$

b) *Range Sensor*: We consider a mobile robot navigating in a planar environment using a 2D range sensor to navigate. We model a 2D range sensor using the range return function  $r: \Phi \rightarrow \mathbb{R}_+$  that returns distances to objects along directions parametrized by angle  $\phi$  from a continuous domain  $\Phi$ . These distances and angles are defined relative to a frame centered at the sensor and fixed to the mobile robot. Note that range  $r$  also depends on the poses of the objects relative to the robot, however we suppress that dependence in the notation for sake of readability. For wheeled robots, we assume the angle  $\phi = 0$  corresponds to the forward heading direction. The domain  $\Phi$  of  $\phi$  depends on each sensor.

## III. PROBLEM STATEMENT

Let  $\mathcal{O}$  be a closed convex subset of  $\mathbb{R}^2$ , and let the distance between the robot at pose  $\mathbf{x}$  and the object at time  $t$  be

$d^*(t)$ . Design a controller that 1) ensures that  $d^*(t) > 0$  for all  $t > 0$  given appropriate initial conditions at  $t = 0$ , 2) ensures that  $v > 0$  for all time, and 3) does not estimate the relative pose of the object to the sensor.

Note that collision avoidance can be guaranteed in a static environment when the robot is motionless; the second part of the problem statement avoids this behavior. All existing guaranteed collision avoidance approaches depend on accurate relative pose information, so that achieving the third part constitutes the contribution of the work.

#### IV. PROPOSED END-TO-END CONTROLLER

To solve the problem in Section III, we propose an end-to-end range-sensor-driven controller. This controller maps a range measurement, or range scan,  $r(\phi)$  to control inputs  $v$  and  $\omega$  of the system. Based on results in [17], [18], we propose using a controller of the form

$$v = v_c e^{-\alpha(\langle w, r \rangle_\Phi)^2}, \text{ and} \quad (2)$$

$$\omega = \langle w, r \rangle_\Phi, \quad (3)$$

where  $\alpha > 0$ ,  $v_c$  is a constant cruise velocity, and  $w: \Phi \rightarrow \mathbb{R}$  is a weight function that parametrizes the functional  $\langle w, r \rangle_\Phi$  with input  $r(\phi)$ . This functional is given by

$$\langle w, r \rangle_\Phi = \int_{\phi \in \Phi} \frac{w(\phi)}{r(\phi)} d\phi, \quad (4)$$

where the weights are given by

$$w(\phi) = -\sin \phi. \quad (5)$$

These weights are zero in the robot's heading. If  $r(\phi)$  is small for  $\phi > 0$ , so that obstacle is to the left of the robot, the robot turns to the right ( $\omega < 0$ ). See Section VII for a discussion on implementation of (4). The reciprocal of the range  $r(\phi)$  is the proximity

$$p(\phi) = \frac{1}{r(\phi)}. \quad (6)$$

The functional in (4) is linear in the proximity scan  $p(\phi)$ .

#### V. GUARANTEED COLLISION AVOIDANCE CONDITIONS

We propose a candidate barrier function defined in a suitable state space related to the relative position between the robot and obstacle, and show that its value increases when the forward velocity  $v$  and angular velocity  $\omega$  satisfy an appropriate inequality. First, we define the state space model.

##### A. Collision Avoidance Kinematics

Given a one-dimensional curve  $\partial\mathcal{O}$  in the plane, we express the relative motion between the robot and object in a frame where one axis is defined by the normal to the object boundary and another is tangent to it. Figure 1 provides an illustration of this frame and the relative pose variables  $\mathbf{x}_S^\mathcal{O} = (s, d^*, \theta)$ , where  $s$  is the arc length along the curve  $\partial\mathcal{O}$ ,  $d^*$  is the distance of the point  $P$  from  $\partial\mathcal{O}$ , and  $\theta$  is the difference between the heading direction of the WMR and the normal to the boundary. The relative pose dynamics

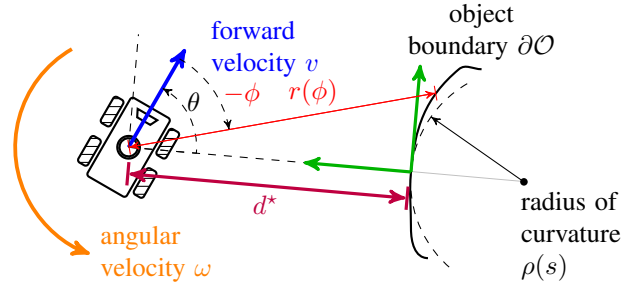


Fig. 1: A wheeled mobile robot with forward speed  $v$ , and angular velocity  $\omega$ . The curved black line represents a local segment of the object boundary  $\partial\mathcal{O}$  with curvature  $\rho$ . A boundary-local frame (green) is also shown. The WMR's state relative to the object consists of the minimum distances  $d^*$  and angle  $\theta$  with respect to the normal to the boundary. The red line shows a lidar return  $r(\phi)$  at a point on  $\partial\mathcal{O}$ , where  $\phi < 0$ .

between mobile robot and object boundary consist of the following equations:

$$\begin{aligned} \dot{s} &= v \sin \theta, \\ \dot{d}^* &= -v \cos \theta, \text{ and} \\ \dot{\theta} &= \omega + \frac{v \sin \theta}{d^* + \rho(s)}, \end{aligned} \quad (7)$$

where  $\rho(s)$  is the object's radius of curvature at the arc length  $s$ ,  $v$  is the forward velocity control input, and  $\omega$  is the angular velocity control input.

##### B. Barrier Function Analysis

The barrier function  $h$  we choose is

$$h(s, d^*, \theta) = |\theta|d^*. \quad (8)$$

**Theorem 1:** Consider a convex object  $\mathcal{O}$  and mobile robot with pose  $\mathbf{x}$  and pose dynamics in (1). Let the relative pose  $\mathbf{x}_S^\mathcal{O}$  satisfy  $0 < |\theta| < \pi/2$ , and  $d^* > 0$ . If

$$\theta\omega > 0 \text{ and } v < 1.5|\omega|d^*, \quad (9)$$

then  $\dot{h} > 0$ , where  $h$  is given in (8).

*Proof.* Let  $s_\theta = \text{sign}(\theta)$ . The time derivative of  $h$  along solutions of (7) is

$$\begin{aligned} \dot{h} &= s_\theta \dot{\theta} d^* + |\theta| \dot{d}^* \\ &= s_\theta \left( \omega + \frac{v \sin \theta}{d^* + \rho(s)} \right) d^* + |\theta|(-v \cos \theta) \\ &= s_\theta \omega d^* + \frac{d^* v s_\theta \sin \theta}{d^* + \rho(s)} - v |\theta| \cos \theta \\ &\geq s_\theta \omega d^* - v |\theta| \cos \theta. \end{aligned}$$

For  $0 < |\theta| < \frac{\pi}{2}$ ,  $0 < |\theta| \cos \theta < 0.5611$ , so that

$$\dot{h} \geq s_\theta \omega d^* - 0.5611v \geq s_\theta \omega d^* - \frac{2}{3}v$$

If  $v < 1.5d^*|\omega|$  and  $\theta\omega > 0$  then  $\dot{h} > 0$ . ■

It is easy to satisfy (9) by designing a state-feedback controller based on tracking the object through  $(d^*, \theta)$ . Our goal is an end-to-end controller that satisfies (9) without explicitly tracking objects, at least when  $d^*$  is small.

## VI. MODELING SENSOR-OBJECT INTERACTIONS

The analysis in Section V provides collision avoidance conditions on  $\omega$  and  $v$ , given the relative pose  $\mathbf{x}_S^O$  of the object with respect to the robot. We need to establish that  $v$  in (2) and  $\omega$  in (3) will result in meeting these conditions even though  $d^*$  and  $\phi^*$  are not estimated. To gain intuition on why this is achievable consider the example of an infinitely long straight wall as the only obstacle:

**Example 1** (Angular velocity due to straight walls): A suitable model for the range scan  $r(\phi)$  due to any wall is

$$r(\phi) = \frac{d^*(\mathbf{x}_S^O)}{\cos(\phi - \phi^*(\mathbf{x}_S^O))} = \frac{d^*}{\cos(\phi - \phi^*)}.$$

Then, using controller (3) with weights (5),  $\omega$  is given by

$$\omega = \int_{\Phi(\mathbf{x}_S^O)} -\sin \phi \frac{\cos(\phi - \phi^*)}{d^*} d\phi = -\frac{\pi}{2} \frac{\sin \phi^*}{d^*} = \frac{\pi \sin \theta}{2 d^*}.$$

Clearly,  $\omega \theta > 0$ . As  $d^* \rightarrow 0$ ,  $|\omega| \rightarrow \infty$ , so that  $v \rightarrow 0$ . Therefore conditions (9) are met for small enough  $d^*$ .

Our main insight is that the convexity of  $\mathcal{O}$ , together with the pose  $\mathbf{x}_S^O$  of the object relative to the robot provide enough information to derive a similar, though conservative, description for the behavior of  $v$  and  $\omega$  near the obstacle.

### A. Range Scans of Convex Objects

This section shows that  $p(\phi) = 1/r(\phi)$  produced by convex objects will be concave enabling characterization of  $\omega$ . First, we characterize objects in terms of their view cones and proximal angles, defined below and seen in Figure 2. We assume that objects are not in collision with the sensor. The object will affect the range scan over an interval  $\Phi(\mathbf{x}_S^O) \subset \Phi$  of angles, which we call the view cone.

**Definition 1** (View Cone): Any object  $\mathcal{O}$  defines an interval  $\Phi(\mathbf{x}_S^O) \subset \Phi$  corresponding to the field-of-view of the object with respect to the sensor. This interval, the *view cone*, corresponds to a cone in  $\mathbb{R}^2$  whose apex is at the sensor. When working in the frame of the sensor, the view cone is given by

$$\Phi(\mathbf{x}_S^O) = \{\phi \in \Phi : \exists t \geq 0 \text{ s.t. } t \begin{bmatrix} \cos \phi \\ \sin \phi \end{bmatrix} \in \mathcal{O}\},$$

where  $t$ , if it exists, is the distance to some point in  $\mathcal{O}$ .

An object that is not in collision with the robot will also possess a non-zero minimum distance to the object. The direction(s) corresponding to this distance constitute the *proximal angle(s)* of the object, which depends on  $\mathbf{x}_S^O$ .

**Definition 2** (Proximal Distance): A proximal distance  $d^*(\mathbf{x}_S^O)$  of an object  $\mathcal{O}$  is given by

$$d^*(\mathbf{x}_S^O) = \min_{\phi \in \Phi(\mathbf{x}_S^O)} r(\phi).$$

**Definition 3** (Proximal Angle): A proximal angle  $\phi^*(\mathbf{x}_S^O)$  of an object  $\mathcal{O}$  is given by

$$\phi^*(\mathbf{x}_S^O) = \arg \min_{\phi \in \Phi(\mathbf{x}_S^O)} r(\phi).$$

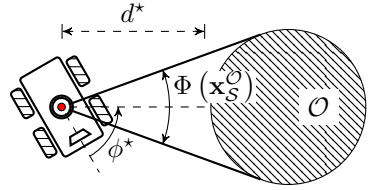


Fig. 2: An object  $\mathcal{O}$  subtends a cone  $\Phi(\mathbf{x}_S^O)$  at the sensor location. The shape of the object produces a unique minimum distance  $d^*$  located at single angle  $\phi^* \in \Phi(\mathbf{x}_S^O)$ .

Note that  $\phi^*(\mathbf{x}_S^O) = -\theta$ . The view cone and proximal angles depend on the shape of the object and its pose relative to the sensor. Convex objects always produce a strictly convex range scan, when not in collision with the sensor. The formal result is below.

**Lemma 1:** Let  $\mathcal{O}$  be convex and compact. Then, for any object pose  $\mathbf{x}_S^O$  where  $x_S \notin \mathcal{O}$

- i)  $\Phi(\mathbf{x}_S^O)$  is compact and connected,
- ii)  $|\Phi(\mathbf{x}_S^O)| \leq \pi$ ,
- iii)  $r(\phi)$  is strictly convex, and
- iv)  $p(\phi)$  is strictly concave.

Note that  $|S|$  for interval  $S \subset \mathbb{R}$  is its width.

*Proof.* The first two claims are direct consequences of the assumption that  $\mathcal{O}$  is convex, compact, and does not contain the sensor origin. The proof focuses on the last two claims.

Any  $\phi^\circ \in \text{Int}(\Phi(\mathbf{x}_S^O))$  defines a unique point  $x^\circ \in \partial\mathcal{O}$ . Let  $L$  be a supporting hyperplane of  $\mathcal{O}$  at  $x^\circ$ . Hyperplane  $L$  separates  $\mathcal{O}$  from  $\mathbf{x}_S^O$ . Let the range scan due to object  $\mathcal{O}$  be  $r(\phi)$ , and the (imaginary) range scan due to  $L$  be  $\underline{r}(\phi)$ . Without loss of generality, one can model a line in the sensor frame as a line  $y = b$  where  $b > 0$  with  $\Phi(\mathbf{x}_S^O) = [0, \pi]$ . The range scan  $\underline{r}(\phi)$  for  $L$  is then given by

$$\underline{r}(\phi) = \frac{b}{\sin \phi} \implies \underline{r}''(\phi) = \underline{r}(\phi) (\cot^2 \phi + 1/\sin^2 \phi) > 0.$$

Therefore,  $\underline{r}(\phi)$  is strictly convex, which implies that

$$\underline{r}(\phi^\circ) + \underline{r}'(\phi^\circ)(\phi - \phi^\circ) < \underline{r}(\phi), \quad (10)$$

for  $\phi \neq \phi^\circ$ . Since  $L$  is a supporting hyperplane to  $\mathcal{O}$  at  $x^\circ$ ,

$$\underline{r}(\phi) \leq r(\phi), \forall \phi \in (0, \pi),$$

$\underline{r}(\phi^\circ) = r(\phi^\circ)$  and  $\underline{r}'(\phi^\circ) = r'(\phi^\circ)$ . We rewrite (10) as

$$r(\phi^\circ) + r'(\phi^\circ)(\phi - \phi^\circ) < \underline{r}(\phi) < r(\phi),$$

for  $\phi \neq \phi^\circ$ . In words,  $r(\phi)$  is strictly convex, for any  $\mathbf{x}_S^O$  not in collision with the sensor.

Let  $\underline{p}(\phi) = 1/r(\phi) = \sin \phi/b$ . Clearly  $\underline{p}''(\phi) < 0$  on  $(0, \pi)$  so that  $\underline{p}(\phi)$  is strictly concave. A similar argument as above implies that  $p(\phi)$  is strictly concave. ■

### B. Characterizing the Angular Velocity

Let  $\theta_e(s, d^*)$  be the angle  $\theta$  at which  $\omega = 0$  for a given location of the robot in the plane relative to the object. For perfectly radially symmetric objects like a circle,  $\theta_e(s, d^*) \equiv 0$ , by resulting symmetry of  $r(\phi)$ . For any other (convex)

object,  $\theta_e(s, d^*)$  is likely non-zero in most states. Hence, generally  $\omega\theta$  is not sign definite. However, if we can bound  $|\theta_e|$ , then we can show that  $\omega\theta > 0$  holds for convex objects when  $|\theta|$  is larger than this bound. We also show that  $|\omega| \rightarrow \infty$  as  $d^* \rightarrow 0$ . Thus we will reach the same conclusions as in Example 1 for any convex object when  $|\theta|$  is large enough.

The bound on  $\theta_e(s, d^*)$  is related to a measure of deviation from radial symmetry which we call the degree of asymmetry (DoA) and denote by  $\bar{\epsilon}(\mathcal{O})$ . A wall's symmetry makes it easy to avoid despite its size; asymmetry introduces confusion in the correct turning direction at small  $\theta$ . To define the DoA, we introduce two inverse functions  $\phi^+(p)$  and  $\phi^-(p)$  of  $p(\phi)$  whose domains are  $\{\phi \in \Phi(\mathbf{x}_S^\mathcal{O}) : \phi > \phi^*\}$  and  $\{\phi \in \Phi(\mathbf{x}_S^\mathcal{O}) : \phi < \phi^*\}$  respectively. These two inverse functions exist because  $p(\phi)$  is strictly concave, by Lemma 1.

**Definition 4** (Local Object Asymmetry Measure): Let  $\mathcal{O}$  be convex. The local object asymmetry measure (LOAM)  $\epsilon$  of  $\mathcal{O}$  at relative pose  $\mathbf{x}_S^\mathcal{O}$  is

$$\epsilon(\mathbf{x}_S^\mathcal{O}) = \max_p |\phi^+(p) + \phi^-(p) - 2\phi^*|.$$

**Definition 5** (Degree of Asymmetry): Let  $\mathcal{O}$  be convex. The degree of asymmetry (DoA)  $\bar{\epsilon}(\mathcal{O})$  of  $\mathcal{O}$  is

$$\bar{\epsilon}(\mathcal{O}) = \max_{\mathbf{x}_S^\mathcal{O}} \epsilon(\mathbf{x}_S^\mathcal{O}).$$

For a circle,  $\bar{\epsilon}(\mathcal{O}) = 0$  by symmetry. For any convex object, since  $|\Phi| \leq \pi$ , therefore  $\bar{\epsilon}(\mathcal{O}) \leq \pi/2$ .

We define the mirrored proximity function  $p_m(\phi)$  as

$$p_m(\phi) = p(-\phi), \quad (11)$$

for  $-\phi \in \Phi(\mathbf{x}_S^\mathcal{O})$ . This function will enable us to bound  $|\omega|$  away from 0 when  $|\phi^*|$  is large enough and in turn derive a bound on  $|\theta_e|$ .

**Lemma 2:** If  $\phi^* \geq \bar{\epsilon}(\mathcal{O})/2$  and  $\phi^-(0) < 0$ , then

$$p_m(\phi) \leq \min(p(\phi), p(0)) \quad \forall \phi \in [0, -\phi^-(0)]. \quad (12)$$

*Proof.* The proof is a formal version of the intuition depicted in Figure 3. Since  $p(\phi)$  is strictly increasing when  $\phi < 0 < \phi^*$ ,  $p_m(\phi)$  is strictly decreasing on  $[0, -\phi^-(0)]$ . Therefore

$$p_m(\phi) \leq p(0) \quad \forall \phi \in [0, -\phi^-(0)]. \quad (13)$$

Moreover, since  $p(\phi)$  is concave,  $p(\phi) \geq p(0)$  on  $[\phi^-(p(0)), \phi^+(p(0))]$  which contains  $[0, \phi^*]$ . In other words,

$$p_m(\phi) \leq p(\phi) \quad \forall \phi \in [0, \phi^*].$$

Combining this bound with (13) we get

$$p_m(\phi) \leq \min(p(\phi), p(0)) \quad \forall \phi \in [0, \min(\phi^*, -\phi^-(0))]. \quad (14)$$

If  $-\phi^-(p(0)) \leq d^*$  we are done. If not, then let  $\phi > \phi^*$ . Since  $\phi^* \geq \bar{\epsilon}(\mathcal{O})/2$ , we have that for all  $p \leq 1/d^*$ ,

$$\begin{aligned} \phi^* &\geq \frac{1}{2} |\phi^+(p) + \phi^-(p) - 2\phi^*| \\ &\implies 2\phi^* \geq \pm (\phi^+(p) + \phi^-(p) - 2\phi^*) \\ &\implies 0 \leq \phi^+(p) + \phi^-(p) \leq 4\phi^*. \end{aligned}$$

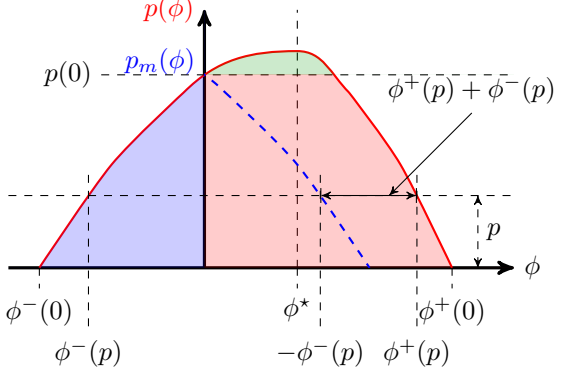


Fig. 3: Assume that  $w(\phi) = -\text{sign}(\phi)$ . The integral  $\langle w, r \rangle_\Phi$  is then the sum of the areas of the red and green regions minus the area of the blue region. The mirrored curve  $p_m(\phi)$  (dashed blue line) will always be below  $p(\phi)$  and  $p(0)$  when  $|\phi^*| > |\bar{\epsilon}|$ , so that area of the red region is always larger than that of the blue region. Therefore, the magnitude of the integral  $\langle w, r \rangle_\Phi$  is lower bounded by the area of the green region. This argument still holds when the weights in  $\langle w, r \rangle_\Phi$  are  $w(\phi) = -\sin \phi$ .

Therefore,

$$\begin{aligned} \phi^+(p_m(\phi)) + \phi^-(p_m(\phi)) &\geq 0 \\ \implies \phi^+(p_m(\phi)) + \phi^-(p(-\phi)) &\geq 0 \\ \implies \phi^+(p_m(\phi)) - \phi &\geq 0. \end{aligned}$$

Since  $\phi > \phi^*$ , and  $p(\phi)$  is strictly decreasing over this range, we must have that

$$p(\phi^+(p_m(\phi))) < p(\phi) \implies p_m(\phi) < p(\phi).$$

Combining this bound with (13) we get

$$p_m(\phi) \leq \min(p(\phi), p(0)) \quad \text{for all } \phi^* < \phi \leq -\phi^-(p(0)). \quad (15)$$

The combination of (14) and (15) completes the proof. ■

**Lemma 3:** If  $\phi^* \leq -\bar{\epsilon}(\mathcal{O})/2$  and  $\phi^+(0) > 0$ , then

$$p_m(\phi) \leq \min(p(\phi), p(0)) \quad \forall \phi \in [-\phi^+(0), 0]. \quad (16)$$

*Proof.* This proof is identical to that of Lemma 2 and hence omitted. ■

The next result generalizes Example 1 to convex objects.

**Lemma 4:** Let  $\mathcal{O}$  be convex with degree of asymmetry  $\bar{\epsilon}(\mathcal{O})$ . If  $\mathbf{x}_S^\mathcal{O}$  is such that  $\frac{\bar{\epsilon}(\mathcal{O})}{2} < |\phi^*| < \frac{\pi}{2}$ , then

- i)  $\langle w, r \rangle_\Phi \phi^* < 0$ , and
- ii)  $|\langle w, r \rangle_\Phi| \geq \frac{(L - \sin L)}{2} \frac{|\sin(\phi^*/2)|}{d^*}$ ,

where  $L = |\Phi_+|$  and

$$\Phi_+ = \{\phi \in \Phi(\mathbf{x}_S^\mathcal{O}) : \phi \phi^* \geq 0, p(\phi) \geq p(0)\}.$$

We consider  $p(0) = 0$  when  $0 \notin \Phi(\mathbf{x}_S^\mathcal{O})$ .

*Proof.* Claim i): If  $0 \notin \Phi(\mathbf{x}_S^\mathcal{O})$  then  $w(\phi)\phi^* < 0$  for all  $\phi \in \Phi(\mathbf{x}_S^\mathcal{O})$ . From the definition of (4) we therefore have that  $\langle w, r \rangle_\Phi \phi^* < 0$ .

Consider the case where  $0 \in \Phi(\mathbf{x}_S^\mathcal{O})$  and  $\phi^* > 0$ , so that

$$\phi^-(0) < 0 \text{ and } \phi^+(0) > 0.$$

We define the extended mirrored proximity scan  $p_{m,ext}(\phi): [0, \phi^+(0)] \rightarrow \mathbb{R}_+$  as

$$p_{m,ext}(\phi) = \begin{cases} p_m(\phi) & \text{if } 0 \leq \phi \leq -\phi^-(0), \\ 0 & \text{if } -\phi^-(0) < \phi \leq \phi^+(0). \end{cases} \quad (17)$$

We divide the integral in (4) into two terms:

$$\langle w, r \rangle_\Phi = \int_{\phi^-(0)}^0 w(\phi)p(\phi)d\phi + \int_0^{\phi^+(0)} w(\phi)p(\phi)d\phi.$$

We rewrite the first term through a temporary change of variable from  $\phi \rightarrow \bar{\phi} = -\phi$ :

$$\begin{aligned} \int_{\phi^-(0)}^0 w(\phi)p(\phi)d\phi &= \int_{-\phi^-(0)}^0 w(-\phi)p(-\phi)(-d\phi) \\ &= - \int_0^{-\phi^-(0)} (-w(\phi))p_m(\phi)(-d\phi) \\ &= - \int_0^{\phi^+(0)} w(\phi)p_{m,ext}(\phi)d\phi, \end{aligned}$$

where we use the definitions of  $p_m(\phi)$  and  $p_{m,ext}(\phi)$  in the above transformation. Given this modified first term, we rewrite  $\langle w, r \rangle_\Phi$ :

$$\langle w, r \rangle_\Phi = \int_0^{\phi^+(0)} w(\phi)(p(\phi) - p_{m,ext}(\phi))d\phi. \quad (18)$$

By construction of  $p_{m,ext}(\phi)$  in (17) and Lemma 2, for the domain of the integral in (18) we have

$$w(\phi) \leq 0 \text{ and } p(\phi) - p_{m,ext}(\phi) \geq 0.$$

Therefore, when  $\phi^* > 0$  then  $\langle w, r \rangle_\Phi < 0$ . An identical argument for the case  $\phi^* < 0$  leads to the conclusion that  $\langle w, r \rangle_\Phi > 0$ . Therefore, these two cases imply the first claim.

Claim ii): We focus on the case where  $\phi^* > \bar{\epsilon}(\mathcal{O})/2 > 0$  and  $0 \in \Phi(\mathbf{x}_S^\mathcal{O})$ . We rewrite (18) by rewriting  $p(\phi)$  as

$$p(\phi) = \max(p(\phi) - p(0), 0) + \min(p(\phi), p(0)),$$

to get an upper bound on the negative quantity  $\langle w, r \rangle_\Phi$ :

$$\begin{aligned} \langle w, r \rangle_\Phi &= \int_0^{\phi^+(0)} w(\phi) [\max(p(\phi) - p(0), 0) \\ &\quad + \min(p(\phi), p(0)) - p_{m,ext}(\phi)] d\phi \\ &= \int_0^{\phi^+(0)} w(\phi) \max(p(\phi) - p(0), 0) d\phi \\ &\quad + \int_0^{\phi^+(0)} w(\phi) [\min(p(\phi), p(0)) - p_{m,ext}(\phi)] d\phi \end{aligned}$$

By Lemma 2, the second integral is non-positive, so that

$$\begin{aligned} \langle w, r \rangle_\Phi &\leq \int_0^{\phi^+(0)} w(\phi) \max(p(\phi) - p(0), 0) d\phi \\ &= \int_{\Phi_+} w(\phi) (p(\phi) - p(0)) d\phi. \end{aligned} \quad (19)$$

This expression captures the intuition that the green region in Figure 3 defines a lower bound for  $|\langle w, r \rangle_\Phi|$ .

By definition of  $\Phi_+$ ,  $p(\phi) - p(0) \geq 0$  for  $\phi \in \Phi_+$ . However,  $p(\phi) - p(0) \equiv 0$  cannot hold since that would imply

$\mathcal{O}$  is non-convex. The smallest we can make this difference given that  $\mathcal{O}$  must be convex is when  $\mathcal{O}$  corresponds to a wall over  $\Phi_+$  with proximal angle as the center of interval  $\Phi_+$  and proximal distance  $d^*$ . An improved bound is therefore

$$p(\phi) - p(0) \geq \frac{\cos(\phi - \phi_m) - \cos(\frac{L}{2})}{d^*},$$

where  $\phi_m$  is the center of interval  $\Phi_+$ . In turn

$$\begin{aligned} \langle w, r \rangle_\Phi &\leq \int_{\Phi_+} w(\phi) \left( \frac{\cos(\phi - \phi_m) - \cos(\frac{L}{2})}{d^*} \right) d\phi \\ &= -\frac{(L - \sin L)}{2} \frac{\sin(\phi_m)}{d^*} \\ &\leq -\frac{(L - \sin L)}{2} \frac{\sin(\phi^*/2)}{d^*}, \end{aligned} \quad (20)$$

where we use the facts that  $\phi_m \geq \phi^*/2$  and  $\sin$  is monotonic on  $[0, \pi/2]$ .

Using identical arguments for the cases where  $\phi^* < -\bar{\epsilon}(\mathcal{O})/2$  and  $0 \notin \Phi(\mathbf{x}_S^\mathcal{O})$ , the proof of claim *ii)* is complete. ■

### C. Main Result

The characterization of  $\langle w, r \rangle_\Phi$ , and therefore  $\omega$ , in Section VI-B leads to the main result.

**Theorem 2:** Consider a convex object  $\mathcal{O}$  with degree of asymmetry  $\bar{\epsilon}(\mathcal{O})$  and mobile robot with pose  $\mathbf{x}$ , pose dynamics in (1), and control (2)-(3). Let the relative pose at time  $t$  be  $\mathbf{x}_S^\mathcal{O}(t) = (s(t), d^*(t), \theta(t))$ . If  $\bar{\epsilon}(\mathcal{O})/2 < |\theta(0)| < \pi/2$  and  $d^*(0) > 0$  then  $d^*(t) > 0$  for all  $t \geq 0$ .

*Proof.* The quantity  $L$  in Lemma 4 monotonically increases with decrease in  $d^*$  up to some finite value. Therefore, for  $\varepsilon > 0$  smaller than this finite value there exists  $\bar{d}_1^* > 0$  such that  $d^* < \bar{d}_1^* \implies L - \sin L > \varepsilon$ . By Lemma 4, if  $d^* < \bar{d}_1^*$  then  $|\langle w, r \rangle_\Phi|d^* = |\omega|d^* > \frac{\varepsilon}{2} \sin\left(\frac{\bar{\epsilon}(\mathcal{O})}{4}\right)$  and  $\theta\omega > 0$ .

Also by Lemma 4,  $|\langle w, r \rangle_\Phi| \rightarrow \infty$  as  $d^* \rightarrow 0$ , so that for  $\alpha > 0$ ,  $v \rightarrow 0$ . Given  $v_c$ ,  $\alpha$  and  $\bar{\epsilon}$ , there exists  $\bar{d}_2^* > 0$  and  $\bar{d}_2^* \leq \bar{d}_1^*$  such that  $v < \frac{\varepsilon}{2} \sin\left(\frac{\bar{\epsilon}(\mathcal{O})}{4}\right)$  for all  $d^* < \bar{d}_2^*$ . Therefore, for  $d^*$  small enough,  $v < 1.5|\omega|d^*$ .

The two paragraphs above and assumptions of this Theorem establish that the conditions for Theorem 1 are met, so that  $\dot{h}(x(t)) > 0$ , where  $h$  is given in (8). By assumption,  $h(x(0)) > 0$ . Therefore, for  $d^*$  small enough,  $h(x(t))$  can never approach zero, so that  $d^*(t)$  can never approach 0. ■

## VII. SIMULATIONS

This section presents simulations of a wheeled mobile robot navigating using 2D LiDAR in an environment with obstacles. Figure 4 depicts this environment along with the trajectories resulting from various initial conditions. The robot successfully avoids the obstacles from multiple initial conditions, without requiring explicit knowledge of either  $d^*$  or  $\phi^*$  for any obstacle. Moreover, some trajectories demonstrate that the controller also avoids non-convex and multiple obstacles, beyond current guarantees.

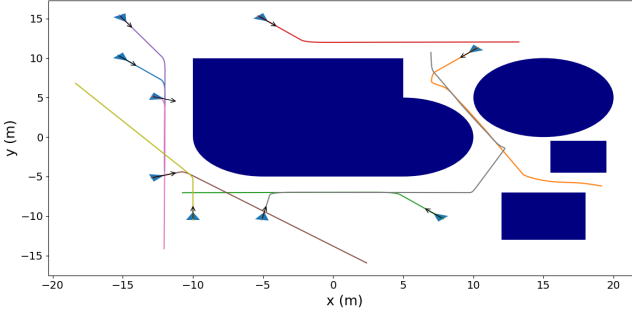


Fig. 4: Top-view of simulated trajectories involving a mobile robot navigating near obstacles (dark blue) without collision. The initial positions are shown using the blue triangles with initial orientations indicated by black arrows.

We use MuJoCo [19] to simulate a custom mobile robot and range sensor. This mobile robot is modeled as a rigid body with two attached wheels that rotate about a common horizontal axis. The wheels accept wheel speed commands  $\omega_r$  and  $\omega_l$ , where the subscripts stand for right and left respectively. Given the control law in (2) and (3), the wheel speeds are simply

$$\omega_r = v + \omega, \text{ and } \omega_l = v - \omega,$$

which ignores the robot wheel base (0.6m) or wheel radii (0.2m). The effect is that the achieved  $v$  and  $\omega$  are scaled versions of the commanded ones, leaving the theory intact.

The LiDAR sensor is 0.6m ahead of the center of the wheel axis. The sensor has a 360° field of view with angular resolution of one degree and a maximum range of 2m. Since the angular resolution is constant, the integral in (4) is implemented as a dot product between the vector of proximity values from the range sensors and a vector of weights defined by (5) at integer values of angles in degrees. The robot starts at a collision-free location and follows the control laws given by (2) with  $\alpha = 1$  and  $v_c = 1\text{m/s}$  and (2) with weights in (5). The actual angular velocity is saturated at 2 rad/s. The simulator physics updates at 500Hz, but the sensor information is updated at only 12.5Hz.

## VIII. DISCUSSION & FUTURE WORK

This paper proposes a method for guaranteed collision avoidance of convex obstacles by a mobile robot. Simulations support the claim. The controller is computationally inexpensive and avoids reliance on feature engineering or learning from data. The work also presents new ideas for modeling and analyzing sensor-object interaction.

*a) Limitations:* First, the claims rely on the relative robot heading being outside an interval, which cannot be *a priori* ensured. For initial conditions inside the interval, collision may occur. Second, it is not clear how to compute or set the values of  $\bar{d}^*_1$  and  $\bar{d}^*_2$ . Third, the guarantees do not address dynamics with bounds on acceleration. A dynamic safety filter that ensures that  $v < 1.5|\omega|d^*$  given commanded  $\omega$  in (3) may be used, but the controller would no longer be end-to-end. Finally, the guarantees do not apply to moving

or multiple obstacles. However, the use of proximity creates an implicit selection mechanism where the robot responds most to the nearest obstacle. This may explain the ability to avoid all obstacles seen in Figure 4.

*b) Future Work:* Future work aims at investigating methods to modify or tune the controller to achieve desired specifications on minimum distances and to meet bounds on linear speed change. Experimental validation is also planned.

## REFERENCES

- [1] D. Fox, W. Burgard, and S. Thrun, “The dynamic window approach to collision avoidance,” *IEEE Robotics & Automation Magazine*, vol. 4, no. 1, pp. 23–33, 1997.
- [2] D. An and H. Wang, “Vph: a new laser radar based obstacle avoidance method for intelligent mobile robots,” in *Fifth World Congress on Intelligent Control and Automation*, vol. 5, 2004, pp. 4681–4685 Vol.5.
- [3] M. Demir and V. Sezer, “Improved follow the gap method for obstacle avoidance,” in *2017 IEEE International Conference on Advanced Intelligent Mechatronics (AIM)*, 2017, pp. 1435–1440.
- [4] J. Zhang, S. Singh, et al., “Loam: Lidar odometry and mapping in real-time.” in *Robotics: Science and systems*, vol. 2, no. 9. Berkeley, CA, 2014, pp. 1–9.
- [5] Z. Liu, X. Liu, and F. Zhang, “Efficient and consistent bundle adjustment on lidar point clouds,” *IEEE Transactions on Robotics*, vol. 39, no. 6, pp. 4366–4386, 2023.
- [6] T.-M. Nguyen, X. Xu, T. Jin, Y. Yang, J. Li, S. Yuan, and L. Xie, “Eigen is all you need: Efficient lidar-inertial continuous-time odometry with internal association,” *IEEE Robotics and Automation Letters*, vol. 9, no. 6, pp. 5330–5337, 2024.
- [7] A. Sridhar, D. Shah, C. Glossop, and S. Levine, “Nomad: Goal masked diffusion policies for navigation and exploration,” in *2024 IEEE International Conference on Robotics and Automation (ICRA)*, 2024, pp. 63–70.
- [8] D. Shah, A. Sridhar, A. Bhorkar, N. Hirose, and S. Levine, “Gnm: A general navigation model to drive any robot,” in *2023 IEEE International Conference on Robotics and Automation (ICRA)*, 2023, pp. 7226–7233.
- [9] J. A. Vincent and M. Schwager, “Reachable polyhedral marching (rpm): An exact analysis tool for deep-learned control systems,” *IEEE Transactions on Neural Networks and Learning Systems*, pp. 1–15, 2025.
- [10] K.-C. Hsu, H. Hu, and J. F. Fisac, “The safety filter: A unified view of safety-critical control in autonomous systems,” *Annual Review of Control, Robotics, and Autonomous Systems*, vol. 7, 2023.
- [11] S. Keyumarsi, M. W. S. Atman, and A. Gusrialdi, “Lidar-based online control barrier function synthesis for safe navigation in unknown environments,” *IEEE Robotics and Automation Letters*, vol. 9, no. 2, pp. 1043–1050, 2024.
- [12] K. Long, C. Qian, J. Cortés, and N. Atanasov, “Learning barrier functions with memory for robust safe navigation,” *IEEE Robotics and Automation Letters*, vol. 6, no. 3, pp. 4931–4938, 2021.
- [13] K. Long, V. Dhiman, M. Leok, J. Cortés, and N. Atanasov, “Safe control synthesis with uncertain dynamics and constraints,” *IEEE Robotics and Automation Letters*, vol. 7, no. 3, pp. 7295–7302, 2022.
- [14] M. Harms, M. Kulkarni, N. Khedekar, M. Jacquet, and K. Alexis, “Neural control barrier functions for safe navigation,” in *2024 IEEE/RSJ International Conference on Intelligent Robots and Systems (IROS)*, 2024, pp. 10415–10422.
- [15] K. Long, Y. Yi, Z. Dai, S. Herbert, J. Cortés, and N. Atanasov, “Sensor-based distributionally robust control for safe robot navigation in dynamic environments,” *The International Journal of Robotics Research*, vol. 0, no. 0, 2025.
- [16] R. Brooks, “A robust layered control system for a mobile robot,” *IEEE Journal on Robotics and Automation*, vol. 2, no. 1, pp. 14–23, 1986.
- [17] B. Clark, V. Hariprasad, and H. A. Poonawala, “Provably correct sensor-driven path-following for unicycles using monotonic score functions,” in *2023 IEEE/RSJ International Conference on Intelligent Robots and Systems (IROS)*, 2023, pp. 354–360.
- [18] B. Clark and H. A. Poonawala, “A monotonicity framework for stability verification of planar path-following controllers,” *IEEE Control Systems Letters*, vol. 8, pp. 406–411, 2024.
- [19] E. Todorov, T. Erez, and Y. Tassa, “MujoCo: A physics engine for model-based control,” in *2012 IEEE/RSJ International Conference on Intelligent Robots and Systems*, 2012, pp. 5026–5033.